Electronic Supplementary Material (ESI) for Journal of Materials Chemistry B.

Supporting Information

3D hollow-out TiO_2 nanowire cluster / GOx as ultrasensitive photoelectrochemical glucose biosensor

Wenke Yang,[a] Xiaohong Wang,[a] Wanjun Hao,[*a] Qiang Wu,[*b] Juan Peng,[c] Jinchun Tu,[a] and Yang Cao,[a,d]

[a] *State Key Laboratory of Marine Resource Utilization in South China Sea, College of Material Science and Engineering, Hainan University, Haikou 570228, China.*

[b] *School of Tropical Medicine and Laboratory Medicine, Key Laboratory of Emergency and Trauma of Ministry of Education, Hainan Medical University, Haikou 571199, China.*

[c] *State Key Laboratory of High-Efficiency Utilization of Coal and Green Chemical Engineering, School of Chemistry and Chemical Engineering, Ningxia University, Yinchuan 750021, China.*

[d] *Qiongtai Normal University, Haikou 571127, China.*

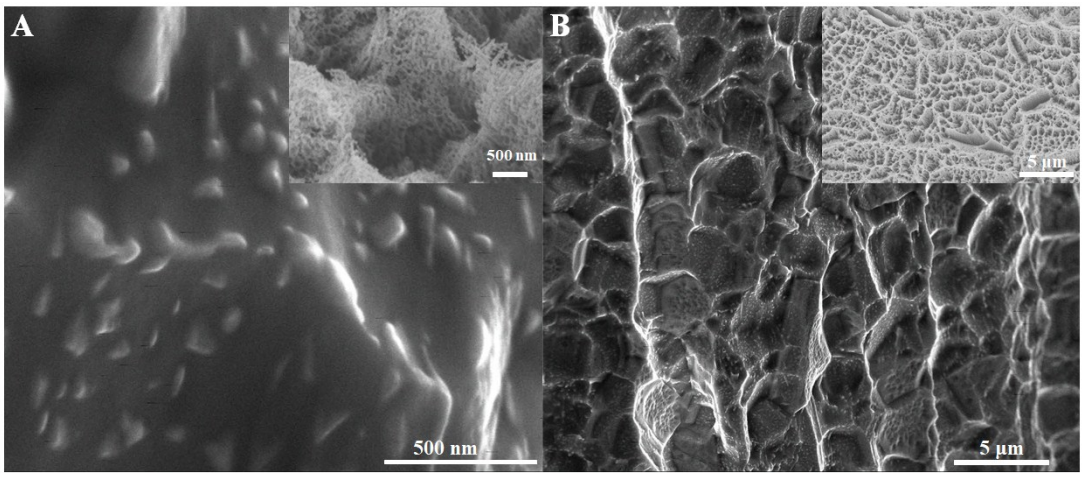

Fig. S1. SEM images (A) and (B) of initial Ti wire mesh at different magnifications. The inset shows the SEM image of the Ti wire mesh after anodization.

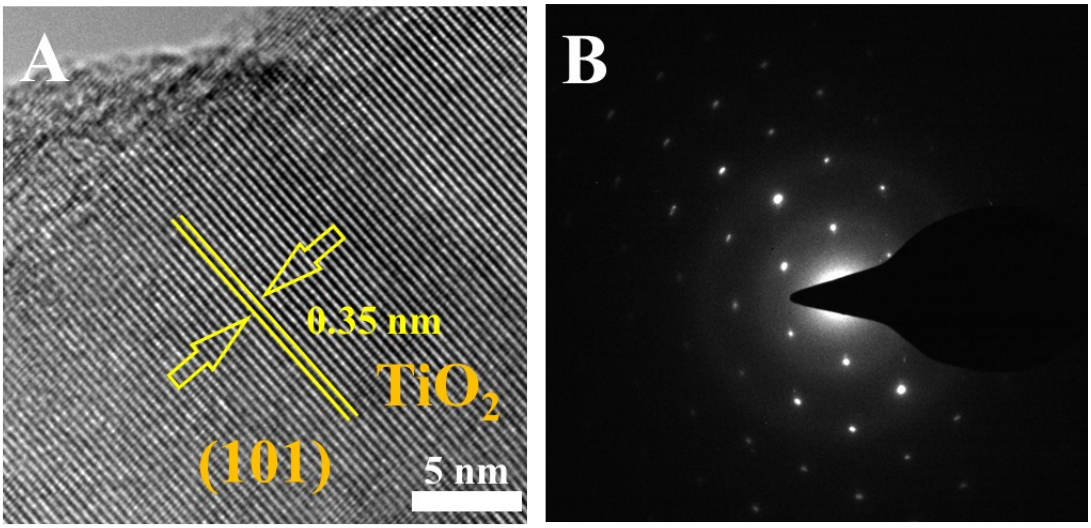

Fig. S2. (A) HR-TEM images of 3D hollow-out TiO_2 NWc of high magnification. (B) SAED pattern of 3D hollow-out TiO_2 NWc.

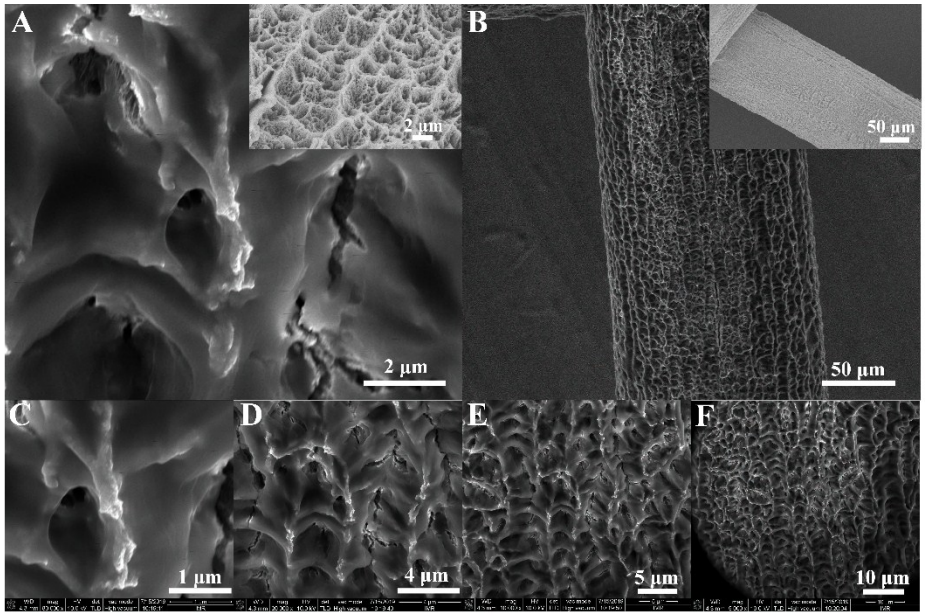

Fig. S3. Partially magnified (A) and complete wire (B) SEM images of 3D hollow-out TiO_2 nanowire cluster loaded with glucose oxidase. SEM images (C, D, E, and F) at different magnifications of 3D hollow-out TiO_2 nanowire cluster after glucose oxidase loading.

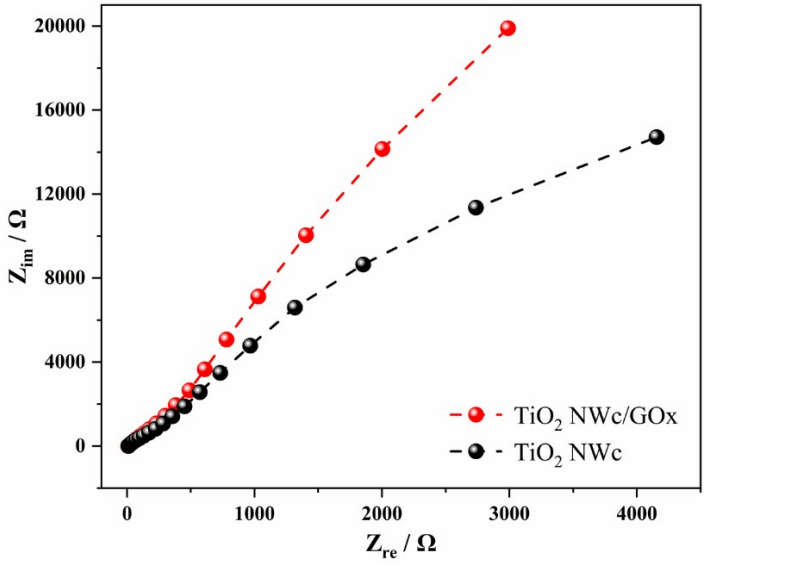

Fig. S4. EIS measurement of TiO_2 NWc before and after GOx loading in 0.1 M PBS (PH=7.4).

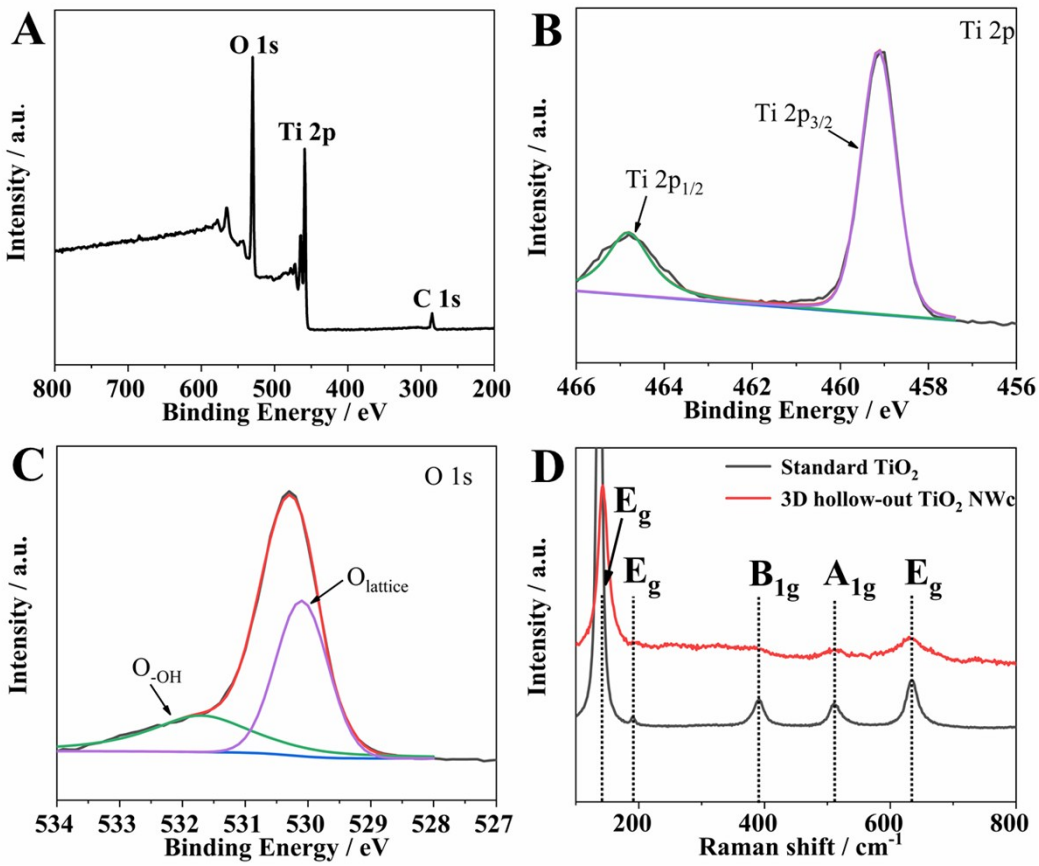

Fig. S5. (A) Wide scan and high-resolution XPS spectra of (B) Ti 2p and (C) O 1s. (D) Raman spectra of 3D hollow-out TiO_2 NWc.

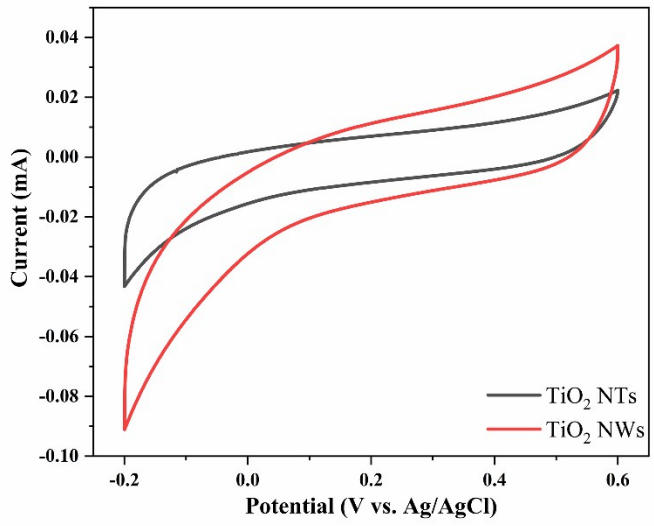

Fig. S6.CV curves for TiO_2 NWc and TiO_2 NTs recorded in 1.0 M PBS (PH=7) at scan rate of 50 mV s^{-1}.

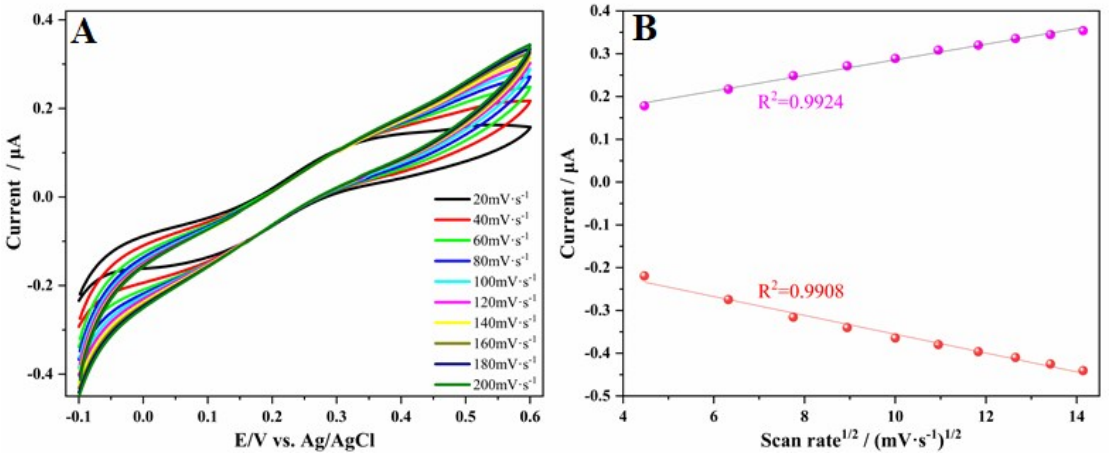

Fig. S7. (A) CV of 3D hollow-out TiO_2 NWc electrode at different scan rates (from 20 $mV \cdot s^{-1}$ to 200 $mV \cdot s^{-1}$) in a solution containing 10 mM of $Fe(CN)_6^{3-/4-}$ (0.1 M KCl). (B) Plots of current versus scan $rate^{1/2}$.

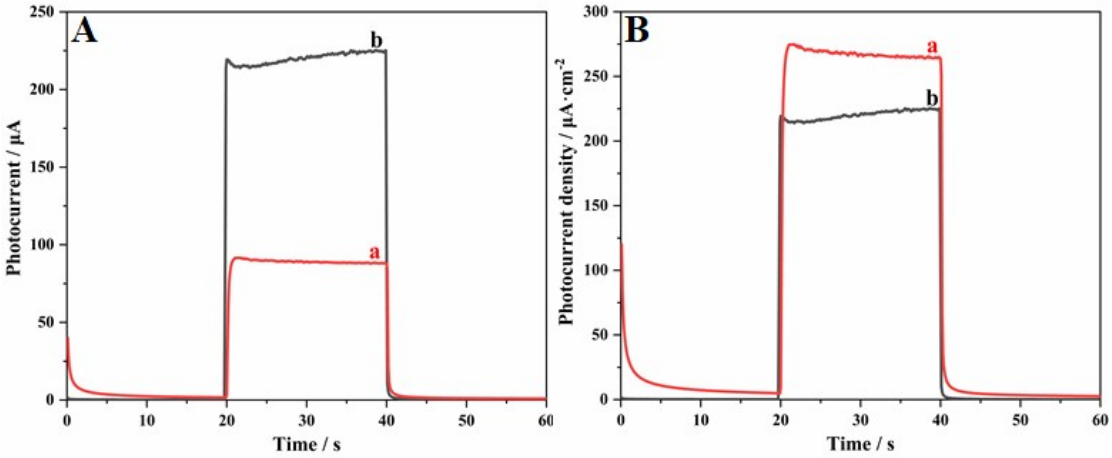

Fig. S8. amperometric i-t curve (A) and time–current density curves (B) of 3D hollow-out TiO_2 NWc (curve a) and TiO_2 NTs (curve b).

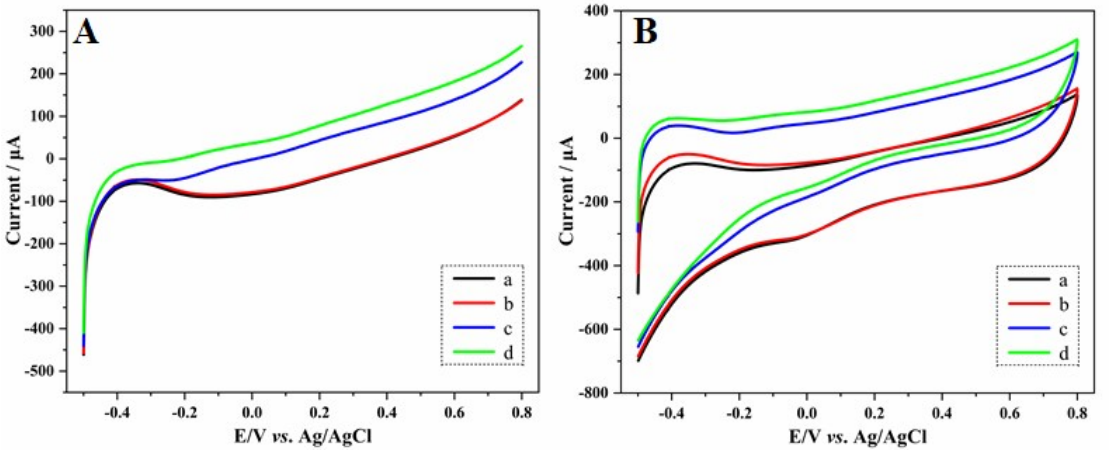

Fig. S9. (A) Linear sweep voltammogram. (B) The CV of the 3D hollow-out TiO_2 NWc

electrode in the (a, c) absence and (b, d) presence of 2 mM glucose under (a, b) lights off and (c, d) on conditions.

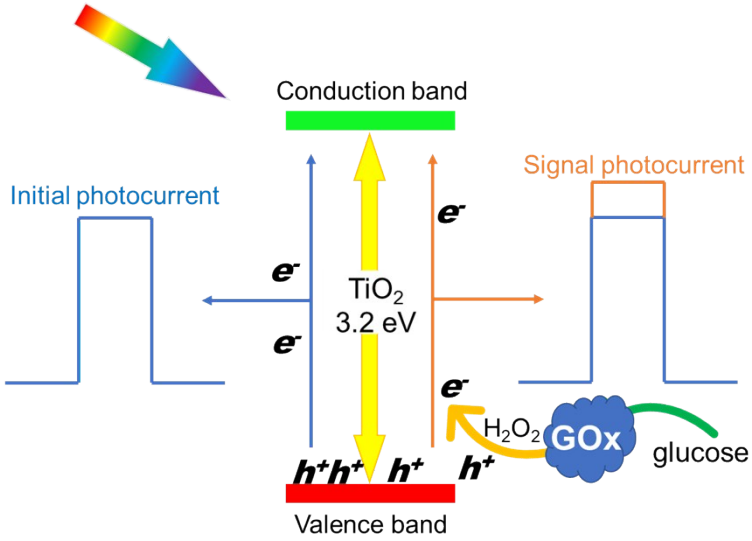

Fig. S10. The mechanism of the photoelectrochemical biosensor.

As shown in Fig. S10, after anatase TiO_2 is irradiated with simulated sunlight, the electrons (e^-) in the valence band absorb the energy of photons and then transition to the conduction band, which forms the initial photocurrent. At the same time, an oxidizing photo-generated hole (h^+) is left in the original position of the electron. In the presence of glucose in the electrolyte, GOx located on the surface of TiO_2 gradually consumes glucose through an enzymatic reaction, thereby generating the active substance H_2O_2. At this time, the photogenerated holes in TiO_2 will capture the enzymatic products to carry out the redox reaction and generate a signal photocurrent. Different glucose concentrations produce variable electrical signals, which convert biological signals into electrical signals.

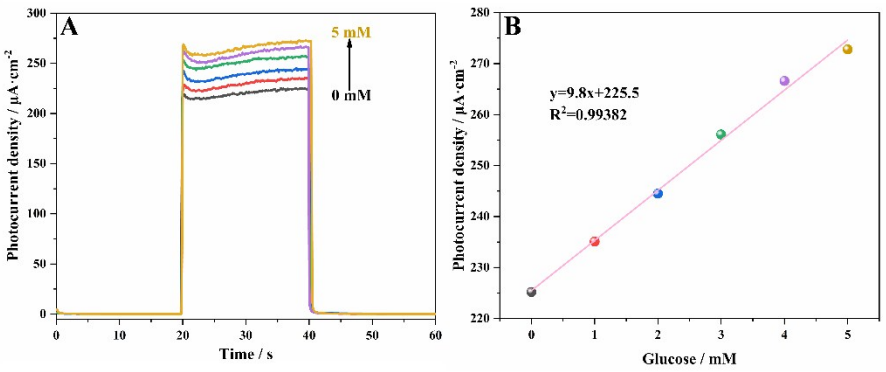

Fig. S11. i–t responses (A) of TiO_2 NTs/GOx toward Glu at increasing concentrations from 0 mM to 5 mM in electrolyte of 0.1 M PBS (pH 7.4). Linear (B) calibration ([Glu] vs. photocurrent density) curves of TiO_2 NTs/GOx biosensor.